


Nonadiabatic Shifting of a Topological Interface in an Electroacoustic Su-Schrieffer-Heeger Lattice

Sai Aditya Raman Kuchibhatla¹ and Michael J. Leamy^{1*}

G. W. Woodruff School of Mechanical Engineering, Georgia Institute of Technology, Atlanta, Georgia 30332, USA

 (Received 3 August 2022; revised 29 September 2022; accepted 21 October 2022; published 18 November 2022)

We investigate numerical and experimental nonadiabatic relocation of a topological interface. We construct a reconfigurable electroacoustic Su-Schrieffer-Heeger lattice using negative-capacitance (NC) shunted piezoelectric patches attached to a host beam. Tuning the NC circuits allows us to create a topological-interface state by varying the effective elastic modulus along the beam. We then use a micro-controller to switch relays placed in the NC shunt circuits to move the interface by one unit cell. We present the results for continuous and pulse inputs and show the shift of energy localization in the experiment. Further, to distinguish topological protection, we simulate the nonadiabatic shifting of a trivial defect in a discrete lattice. Numerical simulations indicate higher mean energy at the interface after shifting a topological state as compared to a defect state. Topological interfaces as shown in our experiment may have interesting applications in acoustic communication, such as source switching and signal encoding.

DOI: [10.1103/PhysRevApplied.18.054058](https://doi.org/10.1103/PhysRevApplied.18.054058)

I. INTRODUCTION

Topologically protected modes (TPMs) are known for their robustness to system disorder, a feature that makes them attractive for applications in quantum computing, photonics, and phononics [1–4]. Numerous studies in the recent literature outline strategies to implement scattering-free waveguiding and lossless transport of information via TPMs in electromagnetic [5], acoustic [6], and elastic [7] media by exploiting analogies with the quantum Hall [8], spin Hall [9], and valley Hall [10] effects. An n -dimensional topological insulator typically supports TPMs to $n - 1$ dimensions. The topological phase-transition phenomena in such systems are explained by models such as the Su-Schrieffer-Heeger (SSH) model [11], the Thouless-Kohmoto-Nightingale-den Nijs (TKNN) model [12], the Haldane model [13], the Kane-Mele model [14], the Bernevig-Hughes-Zhang model [15], and others [1,2].

The SSH model [16] is commonly used to explain the formation of topological edge modes in effectively one-dimensional (1D) systems. Although this model was originally used to explain soliton formation in chains of *trans*-polyacetylene [11], in the past decade it has inspired theoretical and experimental explorations of topological electrical [17,18], photonic [19,20], and acoustic systems [21]. In particular, in acoustics, researchers have demonstrated edge, interface, and corner states in 1D and two-dimensional (2D) SSH structures [21–23]. Further, some have explored the effect of nonlinearities [24–26],

while others have studied spatial and temporal modulation [27–29] of lattice parameters on the appearance of edge or interface modes. Topological edge modes have also been compared to another class of surface states known as Tamm modes [30–33], which occur at the termination of periodic structures. While, in general, Tamm states are not guaranteed topological protection, topological Tamm states have been reported in the literature [34,35].

More recently, in the context of robust information transport, topological pumping of edge states has been actively explored. Inspired by the Thouless pump [36], which describes quantized charge transport, researchers have theoretically studied and experimentally demonstrated the transition of edge states under the action of an external bias [29,37,38]. Notably, topological pumping makes use of an induced parametric variation such that the parameter acts as a virtual dimension, thus bringing, for example, 2D topological effects into 1D systems. For successfully moving the localized energy from one edge to another, topological pumping is required to be adiabatic, wherein the rate of variation of the chosen parameter has an upper bound. Further, to obtain a localization in the middle (instead of the end) of a 1D system, the left and right halves of the system would require different pumping-parameter profiles. Here, to obviate the complexity associated with the addition of a pumping parameter, we explore nonadiabatic shifting of a topological-interface mode in an electroacoustic SSH lattice. Specifically, we demonstrate survival of the interface-amplitude maxima under an instantaneous shift by a unit-cell distance. We anticipate significantly lower energy loss (or decoherence) due to the rapid and highly local change in the presence of

*michael.leafy@me.gatech.edu

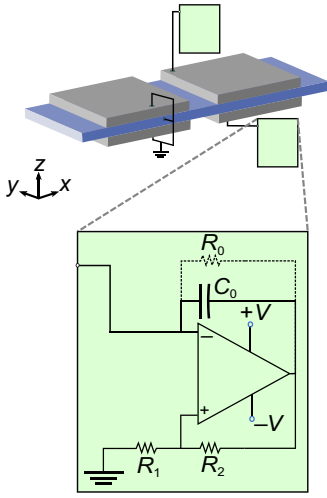


FIG. 1. The unit cell of the reconfigurable electroacoustic SSH beam, showing the negative-capacitance circuit.

topological protection. We present relevant details of the experimental implementation and, by quantitative analysis of the experimentally obtained results, we show the movement of the localized amplitude. We compare the movement of a topological state with a trivial defect state, using numerical simulations to establish the more efficient energy transport in the topological case. We believe that our results may find interesting applications in acoustic communication or acoustic tweezing.

II. RECONFIGURABLE ELECTROACOUSTIC SSH STRUCTURE

Inspired by reconfigurable designs [39,40], we construct the unit cell of the electroacoustic SSH lattice by bonding two pairs of piezoelectric patches (piezos) to a host beam as shown in Fig. 1. Each pair of piezos is symmetrically placed about the host. While one pair of piezos is shorted, the other pair is shunted via a negative-capacitance (NC) circuit [41,42]. The circuitry shown in Fig. 1 reduces the elastic modulus of the connected piezo according to the formula [41]

$$Y = Y_0 \left[1 - \frac{k^2}{(1 + \alpha)} \right]^{-1}, \quad (1)$$

where Y_0 is the short-circuit Young's modulus of the piezo, k is the electromechanical coupling coefficient, and $\alpha = C_{\text{neg}}/C_p$ is the ratio of the NC to the intrinsic capacitance of the piezo. The NC is related to the values of the passive electrical components in the circuit as $C_{\text{neg}} = -C_0 R_2 / R_1$. Typically, a large R_0 is used to ensure circuit stability [43].

We use the effective elastic modulus of the piezos to construct a finite-element model of the unit cell with

only structural elements. We apply periodic boundary conditions and compute the dispersion curves using finite-element analysis [44] to identify a topological band gap. It can be seen from Eq. (1) that the values of α closer to, but less than -1 , lead to a larger difference between the shorted and shunted elastic modulus, which is ideal for larger Bragg band gaps. Specifically, we use $\alpha = -1.15$ with $Y_0 = 84$ GPa and $k = 0.35$, resulting in an effective modulus of $Y = 46$ GPa. These values correspond to the electrical and mechanical parameters used in our experiments. Figure 2(a) shows the dispersion of the longitudinal modes (dashed) and flexural modes (solid lines) with dominant out-of-plane (z -direction) displacement of the unit cell. We identify the Zak phase [45] of the flexural bands surrounding the band gap around 30 kHz, by observing the mode shapes of the inversion-symmetric unit cell at the center and end of the first Brillouin zone [21]. The band possessing the same symmetry for the mode shape has a Zak phase of 0, while that possessing different symmetry has a Zak phase of π [marked in Fig. 2(a); note the mode-shape symmetries]. We find that the Zak phases of the bands surrounding the gap switch (i.e., $\pi \rightarrow 0$ and $0 \rightarrow \pi$) as the shunted and shorted piezos are swapped to make a second type of unit cell. This indicates a topological transition and suggests the presence of an interface mode within the topological band gap [46]. We construct the interface by repeating the two types of unit cells on either side of the interface. By carefully choosing the total number of piezo pairs along the beam, one can ensure that the mode shape at the frequency within the topological gap has amplitude localization only at the interface and not at the termination of the periodic structure. To enable shifting of the interface, we use relays between the piezo and shunt circuits. Switching all the relays between two identified interface positions allows movement of the interface as shown in Fig. 2(b). Note that here we form an interface with neighboring shunted piezos (i.e., effectively soft piezos), as this results in an amplitude maximum in the topological mode and we are interested in shifting this maximum by one unit cell. An interface with neighboring shorted piezos (i.e., stiffer piezos) would result in zero amplitude at the interface, while the maximum amplitude would occur at points half a unit cell away from the interface [33,35]. Later, we show through numerical simulations that both types of interface have topological protection.

III. SHIFTING A TOPOLOGICAL INTERFACE

Figure 2(c) documents the experimental setup detailing the beam with attached piezos. We use a 1.016-mm- (0.04-in.-) thick aluminum host beam to which 24 pairs of rectangular piezos (Steiner and Martins Inc., Davenport, Florida, Part SMPL131W89T10) are vacuum bonded to obtain a 12-unit-cell finite system with unit-cell spacing $a = 30$ cm. The NC shunt circuits are realized using

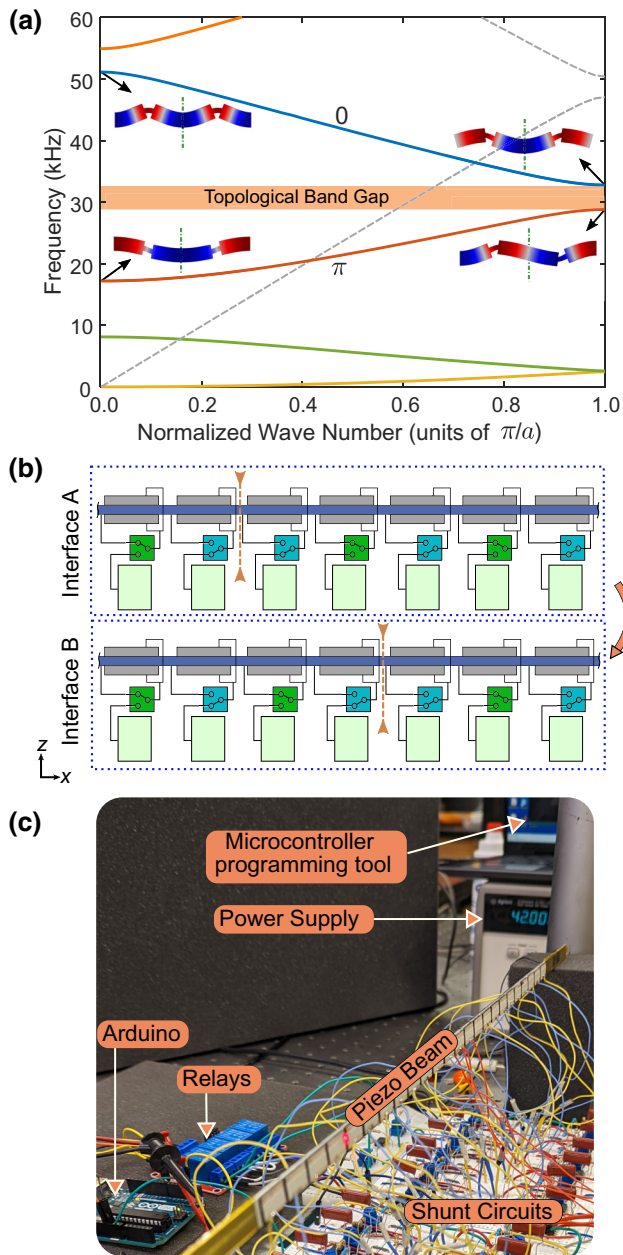


FIG. 2. (a) Dispersion curves of the infinite periodic structure. Only the in-plane flexural modes and longitudinal modes (dashed) are displayed. The mode shapes at the center and end of the Brillouin zone are presented to deduce the Zak phase of the bands. (b) A schematic illustration of moving a topological interface by one unit cell. (c) The experimental setup, depicting the piezo beam along with the required electronics.

OPA445 operational amplifiers and passive components, the nominal values of which are listed in Table I. To accommodate the variation of the capacitance of individual piezos (1.3–1.5 nF), resistance R_2 is constructed with a 10-k Ω analog potentiometer connected in parallel with a 10-k Ω passive resistance. By tuning the potentiometer of each circuit, we obtain an operating point with $\alpha = -1.15$.

TABLE I. Nominal values of the passive electrical elements in the NC shunt circuits used in the experiment.

Label	Value
C_0	1.6 nF
R_1	< 5 k Ω
R_2	4.7 k Ω
R_0	1 M Ω

We use a four-relay module controlled by an Arduino Uno (Arduino LLC, Boston, MA, USA) for timed relocation of the interface by one unit cell. At first, the system is in the “interface-A” configuration, where the interface is located at “location A” ($x = 0$). Switching the relays relocates the interface to “location B” ($x = a$), which results in the “interface-B” configuration [see Fig. 2(b)]. We excite the system by providing an amplified input waveform to a piezo at one end of the beam (near $x = -6a$) and we measure the velocities of points spaced $\frac{1}{2}a$ apart on the beam using a PSV-500 (Polytec GmbH, Waldbronn, Germany) scanning laser Doppler vibrometer (SLDV) at a sampling rate of 250 kHz. We focus our attention on the scan points between $x = 0$ and $x = 6a$ (the end away from the input) to best capture and study the profile of the oscillation amplitude. By providing sinusoidal input at single frequencies between 25 kHz and 35 kHz, we identify 30.5 kHz as a suitable operating frequency for our experiment. Figure 3 shows the amplitude profile of the measured velocity for a harmonic input at 30.5 kHz. The amplitude maximum is observed at the expected locations; i.e., at location A for interface A and location B for interface B, and the decay profile is consistent with that of the topological-interface mode [24,33,35].

Any finite input pulse is dissipated as a consequence of damping in our fabricated system, similar to any other

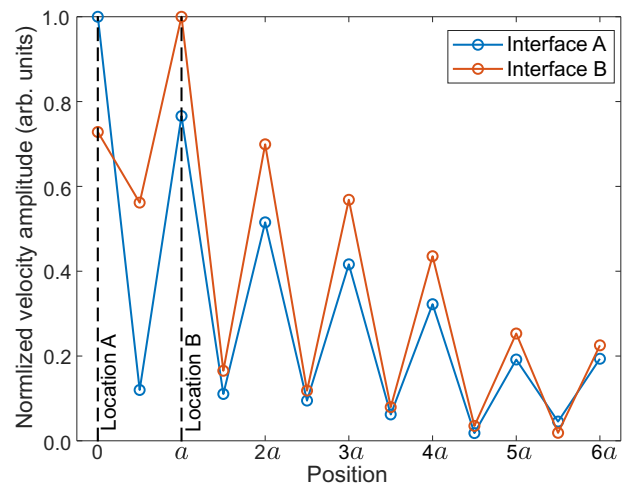


FIG. 3. The profile of the measured velocity amplitude between $x = 0$ and $x = 6a$ for the two interface configurations.

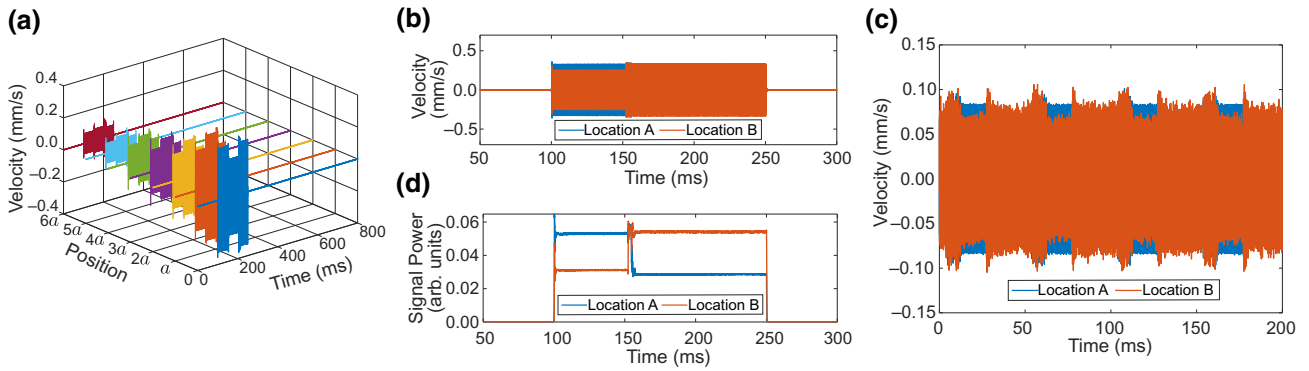


FIG. 4. The measured velocity as the interface is shifted (a) from location A to location B then back to A, (b) from location A to location B once, and (c) between locations A and B every 25 ms. (d) The signal power corresponding to the velocity signals in (b) evaluated in terms of the rms value.

practical structure. Additional damping is expected due to the shunt circuits [47]. For the purpose of studying the response to relocation of the interface, we first look at the case when the interface is relocated before terminating the input. A synchronizing pulse from the SLDV is used to trigger the relays by programming the microcontroller. Figure 4(a) shows the measured velocity at points on one side of the first interface as the beam configuration is changed from interface A to interface B and then back to A before terminating the harmonic input. Accordingly, the amplitude maximum can be seen to move from location A to location B and then back to A. Figure 4(b) shows the velocities measured at locations A and B as the input is provided, starting at $t = 100$ ms, until $t = 250$ ms, while the configuration is switched from interface A to interface B at $t = 150$ ms. The root-mean-square (rms) value of a signal is indicative of the signal power. The rms value of the velocity signal, computed over small windows ($\Delta t = 0.2$ ms), plotted in Fig. 4(c) suggests that the signal power is exchanged as the interface is relocated. The spike in signal power at the instant of switching is attributed to

the step response of the operational amplifiers, resulting in transient dynamics in the beam during which the piezo elastic modulus value settles to a new value. In addition to a finite time delay inherent to the relays used in our experiment, the settling time of the interface modes, which is the time taken for the transient dynamics to dampen out, determines how fast the interface position can be moved. In our experiments, we observe these times to be 2 ms and 1.5 ms, respectively, when moving the interface from location A to location B. Further, the presence of continuous input and proximity to the domain boundary may influence the transient dynamics of the system. Figure 4(d) shows the response to switching the interface between locations A and B every 25 ms, while harmonic input at the topological mode frequency is continuously provided. Clearly, the maximum-amplitude shifts between the two interface locations follow the relocation pattern. The system can thus be used to generate two out-of-phase signals with a single input.

Next, we show that the localized amplitude moves by one unit cell even in the case of finite-duration input. For

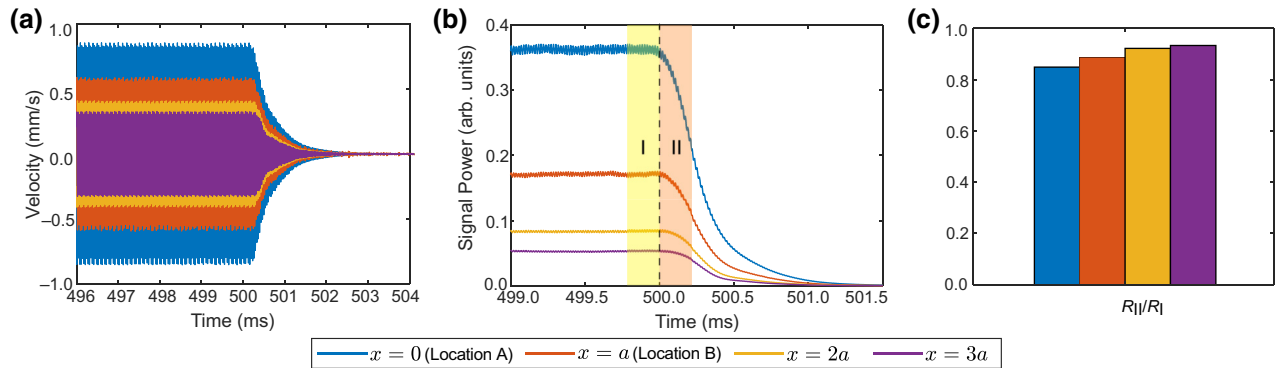


FIG. 5. (a) The measured velocity as the interface is shifted from location A to location B, while the input is terminated simultaneously. (b) The corresponding signal power evaluated in terms of the rms value. (c) The ratio of the signal energy before and after the shift, R_{II}/R_I , computed in a 0.2-ms window marked by labels I and II in (b).

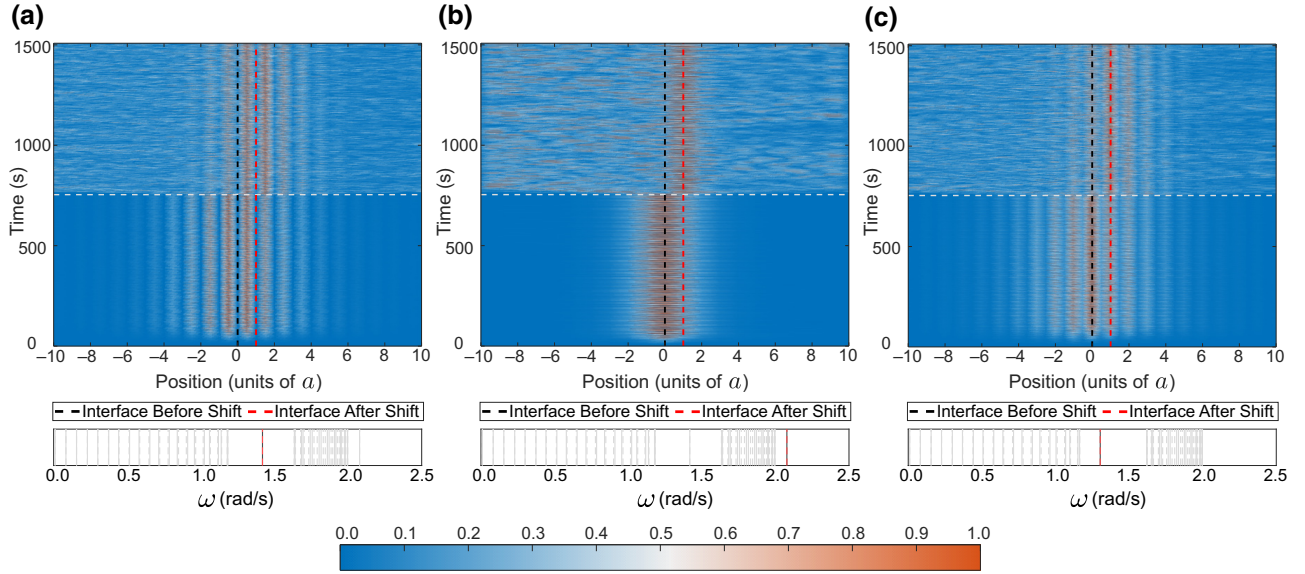


FIG. 6. A numerically simulated temporal map of the displacement amplitude along a discrete lattice on moving (a) a hard interface, (b) a trivial defect, and (c) a soft interface by one unit cell. The bottom panel in each subfigure shows the eigenfrequencies of the finite system in each case while highlighting the topological- or defect-mode frequency.

this purpose, we begin with the configuration in which the interface is at location A, provide input to establish the amplitude localization, and then terminate the input while simultaneously relocating the interface to location B. Figures 5(a) and 5(b) depict the measured velocities and the corresponding signal power [computed similarly to Fig. 4(c)], respectively. Here, the input is exponentially decayed and the interface is moved to location B at $t = 500$ ms. The integral of the signal power gives an estimate of the energy in the signal. To compare the signal energy at various locations before and after the interface shift, we numerically integrate the signal power in a $\Delta t = 0.2$ ms window around the time of shift. The time of shift ($t = 500$ ms) is marked by a dashed vertical line and the windows before and after the shift are labeled as I and II, respectively, in Fig. 5(b). Away from the boundary, we expect the system damping to be uniform and, therefore, any relative increase in the signal energy at a location can be attributed to the interface shifting toward that location. The ratio of the signal energy in the windows $t + \Delta t$ and $t - \Delta t$, referred as R_{II}/R_I , is used as an indicator of the shift in amplitude localization in the beam. Figure 5(c) depicts the value of R_{II}/R_I at $x = 0$, a , $2a$, and $3a$. As the interface is changed to location B, the ratio R_{II}/R_I is higher at location B and subsequent locations in the direction of relocation, thereby confirming the shift of the amplitude maximum in the case of finite input. We wish to emphasize that the value of R_{II}/R_I may vary with experiments depending on the input; however, the trend must remain the same, i.e., the value of the indicator is higher for the location toward which the interface is moving.

IV. TOPOLOGICAL VERSUS TRIVIAL DEFECT

Energy or amplitude localization also occurs at a defect in a periodic structure and the frequency of such a defect mode lies within a band gap. However, in the absence of topological protection, such a defect mode merges into bulk modes with disorder in the system. We anticipate that such a trivial defect mode does not contain the energy very well for a small perturbation at the defect location. To distinguish the advantage of topological modes in the context of moving a defect in periodic structures, we use numerical simulation of oscillations in a finite discrete SSH lattice with unit mass and spring stiffness k_1 (intracell) and k_2 (intercell). We consider a 20-unit-cell open-ended finite periodic system with ten unit cells on either side of an interface (or defect), such that the periodicity is only broken at the interface mass, which is connected to both its neighbors via k_2 . For $k_2 > k_1$, two frequencies can be identified in the eigenvalues of the finite system that fall in the band gap of the periodic structure. One of these is in the topological band gap and we refer to this topological mode as the hard interface, while the other is in the trivial band gap above the optical band of the SSH unit cell and we refer to this as the (trivial) defect mode. For $k_2 < k_1$, only the topological band gap of the periodic system hosts an eigenvalue and we refer to its mode shape as the soft interface. The top panel in Figure 6 shows the absolute displacement along the lattice when a finite pulse at the defect-mode frequency is input at a mass next to the interface and the interface is moved by one unit cell; i.e., from $x = 0$ (vertical black dashed line) to $x = a$ (vertical red dashed line) at the time instance marked by the

horizontal white dashed line. The bottom panels of Fig. 6 depict the eigenfrequencies of the finite structure (the topological or defect mode in color, whereas the bulk modes are in gray), with solid and dashed lines for the system before and after the interface shift. While the topological hard and soft interfaces [Figs. 6(a) and 6(c), respectively] retain the localization profile after the interface shift, the defect mode [Fig. 6(b)] has more energy scattered into the bulk of the structure, which suggests that under nonadiabatic conditions, relocation of a topological state is more robust than of a defect state. We discuss the effect of consecutive relocations in the Supplemental Material [48]. Even though the amount of energy at the new interface location may vary with the system, topological protection ensures more efficient energy transition between topological interfaces compared with trivial defects.

V. CONCLUDING REMARKS

In summary, we experimentally demonstrate the nonadiabatic shifting of a topological interface in an electroacoustic Su-Schrieffer-Heeger beam. The amplitude profile along the beam follows the movement of the interface. The actuation of relays resulting in the shift of the interface is simultaneous with turning off of the input. A trivial defect that also results in localization is not robust under such nonadiabatic shifts [49]. The robustness of topological interfaces on relocation may find interesting applications; for example, in acoustic tweezing to move an object isolated between two interfaces [50] or in acoustic communication by encoding different interface positions.

ACKNOWLEDGMENTS

S.K. thanks Dr. Ahmed Allam and Dr. Christopher Sugino for useful technical discussions related to the fabrication of the piezo-bonded beam and the experimental setup. This material is based upon work supported by the National Science Foundation under Grant No. 1929849. Any opinions, findings, and conclusions or recommendations expressed in this material are those of the author(s) and do not necessarily reflect the views of the National Science Foundation.

[1] M. Z. Hasan and C. L. Kane, Colloquium: Topological insulators, *Rev. Mod. Phys.* **82**, 3045 (2010).
 [2] X.-L. Qi and S.-C. Zhang, Topological insulators and superconductors, *Rev. Mod. Phys.* **83**, 1057 (2011).
 [3] L. Lu, J. D. Joannopoulos, and M. Soljačić, Topological photonics, *Nat. Photonics* **8**, 821 (2014).
 [4] F. Zangeneh-Nejad, A. Alù, and R. Fleury, Topological wave insulators: A review, *C. R. Phys.* **21**, 467 (2020).
 [5] A. B. Khanikaev, S. Hossein Mousavi, W.-K. Tse, M. Kargarian, A. H. MacDonald, and G. Shvets, Photonic topological insulators, *Nat. Mater.* **12**, 233 (2013).

[6] R. Fleury, A. B. Khanikaev, and A. Alu, Floquet topological insulators for sound, *Nat. Commun.* **7**, 1 (2016).
 [7] S. H. Mousavi, A. B. Khanikaev, and Z. Wang, Topologically protected elastic waves in phononic metamaterials, *Nat. Commun.* **6**, 1 (2015).
 [8] K. v. Klitzing, G. Dorda, and M. Pepper, New Method for High-Accuracy Determination of the Fine-Structure Constant Based on Quantized Hall Resistance, *Phys. Rev. Lett.* **45**, 494 (1980).
 [9] C. L. Kane and E. J. Mele, Quantum Spin Hall Effect in Graphene, *Phys. Rev. Lett.* **95**, 226801 (2005).
 [10] A. Rycerz, J. Tworzydło, and C. Beenakker, Valley filter and valley valve in graphene, *Nat. Phys.* **3**, 172 (2007).
 [11] W. Su, J. Schrieffer, and A. J. Heeger, Solitons in Polyacetylene, *Phys. Rev. Lett.* **42**, 1698 (1979).
 [12] D. J. Thouless, M. Kohmoto, M. P. Nightingale, and M. den Nijs, Quantized Hall Conductance in a Two-Dimensional Periodic Potential, *Phys. Rev. Lett.* **49**, 405 (1982).
 [13] F. D. M. Haldane, Model for a Quantum Hall Effect without Landau Levels: Condensed-Matter Realization of the “Parity Anomaly”, *Phys. Rev. Lett.* **61**, 2015 (1988).
 [14] C. L. Kane and E. J. Mele, Z_2 Topological Order and the Quantum Spin Hall Effect, *Phys. Rev. Lett.* **95**, 146802 (2005).
 [15] B. A. Bernevig, T. L. Hughes, and S.-C. Zhang, Quantum spin Hall effect and topological phase transition in HgTe quantum wells, *Science* **314**, 1757 (2006).
 [16] J. K. Asbóth, L. Oroszlány, and A. Pályi, A short course on topological insulators, *Lect. Notes Phys.* **919**, 166 (2016).
 [17] Y. Hadad, J. C. Soric, A. B. Khanikaev, and A. Alu, Self-induced topological protection in nonlinear circuit arrays, *Nat. Electron.* **1**, 178 (2018).
 [18] T. Kotwal, F. Moseley, A. Stegmaier, S. Imhof, H. Brand, T. Kießling, R. Thomale, H. Ronellenfitsch, and J. Dunkel, Active topoelectrical circuits, *Proc. Nat. Acad. Sci.* **118**, e2106411118 (2021).
 [19] G. Cáceres-Aravena, B. Real, D. Guzmán-Silva, A. Amo, L. E. F. Torres, and R. A. Vicencio, Experimental observation of edge states in SSH-stub photonic lattices, *Phys. Rev. Res.* **4**, 013185 (2022).
 [20] C. Jörg, C. Dauer, F. Letscher, M. Fleischhauer, S. Eggert, S. Linden, and G. von Freymann, *et al.*, Limits of topological protection under local periodic driving, *Light: Sci. Appl.* **8**, 1 (2019).
 [21] M. Xiao, G. Ma, Z. Yang, P. Sheng, Z. Zhang, and C. T. Chan, Geometric phase and band inversion in periodic acoustic systems, *Nat. Phys.* **11**, 240 (2015).
 [22] X. Li, Y. Meng, X. Wu, S. Yan, Y. Huang, S. Wang, and W. Wen, Su-Schrieffer-Heeger model inspired acoustic interface states and edge states, *Appl. Phys. Lett.* **113**, 203501 (2018).
 [23] A. Coutant, A. Sivadon, L. Zheng, V. Achilleos, O. Richoux, G. Theocharis, and V. Pagneux, Acoustic Su-Schrieffer-Heeger lattice: Direct mapping of acoustic waveguides to the Su-Schrieffer-Heeger model, *Phys. Rev. B* **103**, 224309 (2021).
 [24] R. K. Pal, J. Vila, M. Leamy, and M. Ruzzene, Amplitude-dependent topological edge states in nonlinear phononic lattices, *Phys. Rev. E* **97**, 032209 (2018).

- [25] R. Chaunsali, H. Xu, J. Yang, P. G. Kevrekidis, and G. Theocharis, Stability of topological edge states under strong nonlinear effects, *Phys. Rev. B* **103**, 024106 (2021).
- [26] R. Chaunsali and G. Theocharis, Self-induced topological transition in phononic crystals by nonlinearity management, *Phys. Rev. B* **100**, 014302 (2019).
- [27] M. I. Rosa, R. K. Pal, J. R. Arruda, and M. Ruzzene, Edge States and Topological Pumping in Spatially Modulated Elastic Lattices, *Phys. Rev. Lett.* **123**, 034301 (2019).
- [28] E. Riva, M. I. Rosa, and M. Ruzzene, Edge states and topological pumping in stiffness-modulated elastic plates, *Phys. Rev. B* **101**, 094307 (2020).
- [29] Y. Xia, E. Riva, M. I. Rosa, G. Cazzulani, A. Erturk, F. Braghin, and M. Ruzzene, Experimental Observation of Temporal Pumping in Electromechanical Waveguides, *Phys. Rev. Lett.* **126**, 095501 (2021).
- [30] Z. He, S. Peng, M. Ke, J. Shi, K. Deng, H. Zhao, Z. Liu, W. Wen, and P. Sheng, Acoustic surface-guided modes in phononic crystals, *EPL (Europhys. Lett.)* **104**, 34005 (2013).
- [31] H.-X. Wang, C. Liang, Y. Poo, P.-G. Luan, and G.-Y. Guo, The topological edge modes and tamm modes in Su-Schrieffer-Heeger LC-resonator circuits, *J. Phys. D: Appl. Phys.* **54**, 435301 (2021).
- [32] D. Liao, Z. Yue, Z. Zhang, H.-X. Wang, Y. Cheng, and X. Liu, Observations of Tamm modes in acoustic topological insulators, *Appl. Phys. Lett.* **120**, 211701 (2022).
- [33] T. Chen, Y. Yu, Y. Song, D. Yu, H. Ye, J. Xie, X. Shen, Y. Pan, and Q. Cheng, Distinguishing the topological zero mode and Tamm mode in a microwave waveguide array, *Ann. Phys.* **531**, 1900347 (2019).
- [34] J. Henriques, T. Rappoport, Y. V. Bludov, M. Vasilevskiy, and N. Peres, Topological photonic Tamm states and the Su-Schrieffer-Heeger model, *Phys. Rev. A* **101**, 043811 (2020).
- [35] L. Wang, W. Cai, M. Bie, X. Zhang, and J. Xu, Zak phase and topological plasmonic Tamm states in one-dimensional plasmonic crystals, *Opt. Express* **26**, 28963 (2018).
- [36] D. Thouless, Quantization of particle transport, *Phys. Rev. B* **27**, 6083 (1983).
- [37] I. H. Grinberg, M. Lin, C. Harris, W. A. Benalcazar, C. W. Peterson, T. L. Hughes, and G. Bahl, Robust temporal pumping in a magneto-mechanical topological insulator, *Nat. Commun.* **11**, 1 (2020).
- [38] W. Cheng, E. Prodan, and C. Prodan, Experimental Demonstration of Dynamic Topological Pumping across Incommensurate Bilayered Acoustic Metamaterials, *Phys. Rev. Lett.* **125**, 224301 (2020).
- [39] A. Darabi, M. Collet, and M. J. Leamy, Experimental realization of a reconfigurable electroacoustic topological insulator, *Proc. Nat. Acad. Sci.* **117**, 16138 (2020).
- [40] A. Darabi, E. Kliewer, and M. J. Leamy, Reconfigurable acoustic multiplexer/demultiplexer using time division, *Appl. Phys. Lett.* **119**, 113501 (2021).
- [41] M. Date, M. Kutani, and S. Sakai, Electrically controlled elasticity utilizing piezoelectric coupling, *J. Appl. Phys.* **87**, 863 (2000).
- [42] E. Fukada, M. Date, K. Kimura, T. Okubo, H. Kodama, P. Mokry, and K. Yamamoto, Sound isolation by piezoelectric polymer films connected to negative capacitance circuits, *IEEE Trans. Dielectr. Electr. Insul.* **11**, 328 (2004).
- [43] J. Marconi, E. Riva, M. Di Ronco, G. Cazzulani, F. Braghin, and M. Ruzzene, Experimental Observation of Nonreciprocal Band Gaps in a Space-Time-Modulated Beam Using a Shunted Piezoelectric Array, *Phys. Rev. Appl.* **13**, 031001 (2020).
- [44] COMSOL MULTIPHYSICS®v. 5.5, www.comsol.com, COMSOL AB, Stockholm, Sweden.
- [45] J. Zak, Berry's Phase for Energy Bands in Solids, *Phys. Rev. Lett.* **62**, 2747 (1989).
- [46] M. Xiao, Z. Zhang, and C. T. Chan, Surface Impedance and Bulk Band Geometric Phases in One-Dimensional Systems, *Phys. Rev. X* **4**, 021017 (2014).
- [47] N. W. Hagood and A. Von Flotow, Damping of structural vibrations with piezoelectric materials and passive electrical networks, *J. Sound Vib.* **146**, 243 (1991).
- [48] See the Supplemental Material at <http://link.aps.org/supplemental/10.1103/PhysRevApplied.18.054058> for a brief discussion on consecutive relocations of the interface.
- [49] R. L. Thomes, D. Beli, and C. De Marqui Jr., Space-time wave localization in electromechanical metamaterial beams with programmable defects, *Mech. Syst. Signal Process.* **167**, 108550 (2022).
- [50] C. Schmidt, A. Palatnik, M. Sudzius, S. Meister, and K. Leo, Coupled topological interface states, *Phys. Rev. B* **103**, 085412 (2021).